Eur. Phys. J. C 2, 61–75 (1998)

THE EUROPEAN PHYSICAL JOURNAL C

Measurement of jet shapes in photoproduction at HERA

ZEUS Collaboration

J. Breitweg, M. Derrick, D. Krakauer, S. Magill, D. Mikunas, B. Musgrave, J. Repond, R. Stanek, R.L. Talaga, R. Yoshida, H. Zhang

Argonne National Laboratory, Argonne, IL, USA [p]

M.C.K. Mattingly

Andrews University, Berrien Springs, MI, USA

F. Anselmo, P. Antonioli, G. Bari, M. Basile, L. Bellagamba, D. Boscherini, A. Bruni, G. Bruni, G. Cara Romeo, G. Castellini[1], L. Cifarelli[2], F. Cindolo, A. Contin, M. Corradi, S. De Pasquale, I. Gialas[3], P. Giusti, G. Iacobucci, G. Laurenti, G. Levi, A. Margotti, T. Massam, R. Nania, F. Palmonari, A. Pesci, A. Polini, F. Ricci, G. Sartorelli, Y. Zamora Garcia[4], A. Zichichi

University and INFN Bologna, Bologna, Italy [f]

C. Amelung, A. Bornheim, I. Brock, K. Coböken, J. Crittenden, R. Deffner, M. Eckert, M. Grothe, H. Hartmann, K. Heinloth, L. Heinz, E. Hilger, H.-P. Jakob, U.F. Katz, R. Kerger, E. Paul, M. Pfeiffer, Ch. Rembser[5], J. Stamm, R. Wedemeyer[6], H. Wieber

Physikalisches Institut der Universität Bonn, Bonn, Germany [c]

D.S. Bailey, S. Campbell-Robson, W.N. Cottingham, B. Foster, R. Hall-Wilton, M.E. Hayes, G.P. Heath, H.F. Heath, J.D. McFall, D. Piccioni, D.G. Roff, R.J. Tapper

H.H. Wills Physics Laboratory, University of Bristol, Bristol, U.K. [o]

M. Arneodo[7], R. Ayad, M. Capua, A. Garfagnini, L. Iannotti, M. Schioppa, G. Susinno

Calabria University, Physics Department and INFN, Cosenza, Italy [f]

J.Y. Kim, J.H. Lee, I.T. Lim, M.Y. Pac[8]

Chonnam National University, Kwangju, Korea [h]

A. Caldwell[9], N. Cartiglia, Z. Jing, W. Liu, B. Mellado, J.A. Parsons, S. Ritz[10], S. Sampson, F. Sciulli, P.B. Straub, Q. Zhu

Columbia University, Nevis Labs., Irvington on Hudson, N.Y., USA [q]

P. Borzemski, J. Chwastowski, A. Eskreys, J. Figiel, K. Klimek, M.B. Przybycień, L. Zawiejski

Institute of Nuclear Physics, Cracow, Poland [j]

L. Adamczyk[11], B. Bednarek, M. Bukowy, K. Jeleń, D. Kisielewska, T. Kowalski, M. Przybycień, E. Rulikowska-Zarębska, L. Suszycki, J. Zając

Faculty of Physics and Nuclear Techniques, Academy of Mining and Metallurgy, Cracow, Poland [j]

Z. Duliński, A. Kotański

Jagellonian University, Department of Physics, Cracow, Poland [k]

G. Abbiendi[12], L.A.T. Bauerdick, U. Behrens, H. Beier, J.K. Bienlein, G. Cases[13], O. Deppe, K. Desler, G. Drews, U. Fricke, D.J. Gilkinson, C. Glasman, P. Göttlicher, T. Haas, W. Hain, D. Hasell, K.F. Johnson[14], M. Kasemann, W. Koch, U. Kötz, H. Kowalski, J. Labs, L. Lindemann, B. Löhr, M. Löwe[15], O. Mańczak, J. Milewski,

T. Monteiro[16], J.S.T. Ng[17], D. Notz, K. Ohrenberg[18], I.H. Park[19], A. Pellegrino, F. Pelucchi, K. Piotrzkowski, M. Roco[20], M. Rohde, J. Roldán, J.J. Ryan, A.A. Savin, U. Schneekloth, F. Selonke, B. Surrow, E. Tassi, T. Voß[21], D. Westphal, G. Wolf, U. Wollmer[22], C. Youngman, A.F. Żarnecki, W. Zeuner

Deutsches Elektronen-Synchrotron DESY, Hamburg, Germany

B.D. Burow, H.J. Grabosch, A. Meyer, S. Schlenstedt

DESY-IfH Zeuthen, Zeuthen, Germany

G. Barbagli, E. Gallo, P. Pelfer

University and INFN, Florence, Italy [f]

G. Maccarrone, L. Votano

INFN, Laboratori Nazionali di Frascati, Frascati, Italy [f]

A. Bamberger, S. Eisenhardt, P. Markun, T. Trefzger[23], S. Wölfle

Fakultät für Physik der Universität Freiburg i.Br., Freiburg i.Br., Germany [c]

J.T. Bromley, N.H. Brook, P.J. Bussey, A.T. Doyle, N. Macdonald, D.H. Saxon, L.E. Sinclair, E. Strickland, R. Waugh

Department of Physics and Astronomy, University of Glasgow, Glasgow, U.K. [o]

I. Bohnet, N. Gendner, U. Holm, A. Meyer-Larsen, H. Salehi, K. Wick

Hamburg University, I. Institute of Exp. Physics, Hamburg, Germany [c]

L.K. Gladilin[24], D. Horstmann, D. Kçira, R. Klanner, E. Lohrmann, G. Poelz, W. Schott[25], F. Zetsche

Hamburg University, II. Institute of Exp. Physics, Hamburg, Germany [c]

T.C. Bacon, I. Butterworth, J.E. Cole, G. Howell, B.H.Y. Hung, L. Lamberti[26], K.R. Long, D.B. Miller, N. Pavel, A. Prinias[27], J.K. Sedgbeer, D. Sideris

Imperial College London, High Energy Nuclear Physics Group, London, U.K. [o]

U. Mallik, S.M. Wang, J.T. Wu

University of Iowa, Physics and Astronomy Department, Iowa City, USA [p]

P. Cloth, D. Filges

Forschungszentrum Jülich, Institut für Kernphysik, Jülich, Germany

J.I. Fleck[5], T. Ishii, M. Kuze, I. Suzuki[28], K. Tokushuku, S. Yamada, K. Yamauchi, Y. Yamazaki[29]

Institute of Particle and Nuclear Studies, KEK, Tsukuba, Japan [g]

S.J. Hong, S.B. Lee, S.W. Nam[30], S.K. Park

Korea University, Seoul, Korea [h]

F. Barreiro, J.P. Fernández, G. García, R. Graciani, J.M. Hernández, L. Hervás[5], L. Labarga, M. Martínez, J. del Peso, J. Puga, J. Terrón[31], J.F. de Trocóniz

Universidad Autónoma Madrid, Depto de Física Teórica, Madrid, Spain [n]

F. Corriveau, D.S. Hanna, J. Hartmann, L.W. Hung, W.N. Murray, A. Ochs, M. Riveline, D.G. Stairs, M. St-Laurent, R. Ullmann

McGill University, Department of Physics, Montréal, Québec, Canada [a], [b]

T. Tsurugai

Meiji Gakuin University, Faculty of General Education, Yokohama, Japan

V. Bashkirov, B.A. Dolgoshein, A. Stifutkin
Moscow Engineering Physics Institute, Moscow, Russia [l]

G.L. Bashindzhagyan, P.F. Ermolov, Yu.A. Golubkov, L.A. Khein, N.A. Korotkova, I.A. Korzhavina, V.A. Kuzmin, O.Yu. Lukina, A.S. Proskuryakov, L.M. Shcheglova[32], A.N. Solomin[32], S.A. Zotkin
Moscow State University, Institute of Nuclear Physics, Moscow, Russia [m]

C. Bokel, M. Botje, N. Brümmer, F. Chlebana[20], J. Engelen, E. Koffeman, P. Kooijman, A. van Sighem, H. Tiecke, N. Tuning, W. Verkerke, J. Vossebeld, M. Vreeswijk[5], L. Wiggers, E. de Wolf
NIKHEF and University of Amsterdam, Amsterdam, Netherlands [i]

D. Acosta, B. Bylsma, L.S. Durkin, J. Gilmore, C.M. Ginsburg, C.L. Kim, T.Y. Ling, P. Nylander, T.A. Romanowski[33]
Ohio State University, Physics Department, Columbus, Ohio, USA [p]

H.E. Blaikley, R.J. Cashmore, A.M. Cooper-Sarkar, R.C.E. Devenish, J.K. Edmonds, J. Große-Knetter[34], N. Harnew, C. Nath, V.A. Noyes[35], A. Quadt, O. Ruske, J.R. Tickner[27], H. Uijterwaal, R. Walczak, D.S. Waters
Department of Physics, University of Oxford, Oxford, U.K. [o]

A. Bertolin, R. Brugnera, R. Carlin, F. Dal Corso, U. Dosselli, S. Limentani, M. Morandin, M. Posocco, L. Stanco, R. Stroili, C. Voci
Dipartimento di Fisica dell' Università and INFN, Padova, Italy [f]

J. Bulmahn, B.Y. Oh, J.R. Okrasiński, W.S. Toothacker, J.J. Whitmore
Pennsylvania State University, Department of Physics, University Park, PA, USA [q]

Y. Iga
Polytechnic University, Sagamihara, Japan [g]

G. D'Agostini, G. Marini, A. Nigro, M. Raso
Dipartimento di Fisica, Univ. 'La Sapienza' and INFN, Rome, Italy [f]

J.C. Hart, N.A. McCubbin, T.P. Shah
Rutherford Appleton Laboratory, Chilton, Didcot, Oxon, U.K. [o]

D. Epperson, C. Heusch, J.T. Rahn, H.F.-W. Sadrozinski, A. Seiden, R. Wichmann, D.C. Williams
University of California, Santa Cruz, CA, USA [p]

O. Schwarzer, A.H. Walenta
Fachbereich Physik der Universität-Gesamthochschule Siegen, Germany [c]

H. Abramowicz[36], G. Briskin, S. Dagan[36], S. Kananov[36], A. Levy[36]
Raymond and Beverly Sackler Faculty of Exact Sciences, School of Physics, Tel-Aviv University, Tel-Aviv, Israel [e]

T. Abe, T. Fusayasu, M. Inuzuka, K. Nagano, K. Umemori, T. Yamashita
Department of Physics, University of Tokyo, Tokyo, Japan [g]

R. Hamatsu, T. Hirose, K. Homma[37], S. Kitamura[38], T. Matsushita
Tokyo Metropolitan University, Department of Physics, Tokyo, Japan [g]

R. Cirio, M. Costa, M.I. Ferrero, S. Maselli, V. Monaco, C. Peroni, M.C. Petrucci, M. Ruspa, R. Sacchi, A. Solano, A. Staiano
Università di Torino, Dipartimento di Fisica Sperimentale and INFN, Torino, Italy [f]

M. Dardo
II Faculty of Sciences, Torino University and INFN - Alessandria, Italy [f]

D.C. Bailey, C.-P. Fagerstroem, R. Galea, G.F. Hartner, K.K. Joo, G.M. Levman, J.F. Martin, R.S. Orr, S. Polenz, A. Sabetfakhri, D. Simmons, R.J. Teuscher[5]
University of Toronto, Department of Physics, Toronto, Ont., Canada [a]

J.M. Butterworth, C.D. Catterall, T.W. Jones, J.B. Lane, R.L. Saunders, M.R. Sutton, M. Wing
University College London, Physics and Astronomy Department, London, U.K. [o]

J. Ciborowski, G. Grzelak[39], M. Kasprzak, K. Muchorowski[40], R.J. Nowak, J.M. Pawlak, R. Pawlak, T. Tymieniecka, A.K. Wróblewski, J.A. Zakrzewski
Warsaw University, Institute of Experimental Physics, Warsaw, Poland [j]

M. Adamus
Institute for Nuclear Studies, Warsaw, Poland [j]

C. Coldewey, Y. Eisenberg[36], D. Hochman, U. Karshon[36]
Weizmann Institute, Department of Particle Physics, Rehovot, Israel [d]

W.F. Badgett, D. Chapin, R. Cross, S. Dasu, C. Foudas, R.J. Loveless, S. Mattingly, D.D. Reeder, W.H. Smith, A. Vaiciulis, M. Wodarczyk
University of Wisconsin, Department of Physics, Madison, WI, USA [p]

S. Bhadra, W.R. Frisken, M. Khakzad, W.B. Schmidke
York University, Department of Physics, North York, Ont., Canada [a]

Received: 30 September 1997

Abstract. The shape of jets produced in quasi-real photon-proton collisions at centre-of-mass energies in the range 134–277 GeV has been measured using the hadronic energy flow. The measurement was done with the ZEUS detector at HERA. Jets are identified using a cone algorithm in the $\eta - \phi$ plane with a cone radius of one unit. Measured jet shapes both in inclusive jet and dijet production with transverse energies $E_T^{jet} > 14$ GeV are presented. The jet shape broadens as the jet pseudorapidity (η^{jet}) increases and narrows as E_T^{jet} increases. In dijet photoproduction, the jet shapes have been measured separately for samples dominated by resolved and by direct processes. Leading-logarithm parton-shower Monte Carlo calculations of resolved and direct processes describe well the measured jet shapes except for the inclusive production of jets with high η^{jet} and low E_T^{jet}. The observed broadening of the jet shape as η^{jet} increases is consistent with the predicted increase in the fraction of final state gluon jets.

[1] also at IROE Florence, Italy
[2] now at Univ. of Salerno and INFN Napoli, Italy
[3] now at Univ. of Crete, Greece
[4] supported by Worldlab, Lausanne, Switzerland
[5] now at CERN
[6] retired
[7] also at University of Torino and Alexander von Humboldt Fellow at DESY
[8] now at Dongshin University, Naju, Korea
[9] also at DESY
[10] Alfred P. Sloan Foundation Fellow
[11] supported by the Polish State Committee for Scientific Research, grant No. 2P03B14912
[12] supported by an EC fellowship number ERBFMBICT 950172
[13] now at SAP A.G., Walldorf
[14] visitor from Florida State University
[15] now at ALCATEL Mobile Communication GmbH, Stuttgart
[16] supported by European Community Program PRAXIS XXI
[17] now at DESY-Group FDET
[18] now at DESY Computer Center
[19] visitor from Kyungpook National University, Taegu, Korea, partially supported by DESY
[20] now at Fermi National Accelerator Laboratory (FNAL), Batavia, IL, USA
[21] now at NORCOM Infosystems, Hamburg
[22] now at Oxford University, supported by DAAD fellowship HSP II-AUFE III
[23] now at ATLAS Collaboration, Univ. of Munich
[24] on leave from MSU, supported by the GIF, contract I-0444-

1 Introduction

Photoproduction at HERA is studied via ep scattering at low four-momentum transfers ($Q^2 \approx 0$, where Q^2 is the virtuality of the exchanged photon). In photon-proton reactions, two types of QCD processes contribute to jet production at leading order (LO) [1,2]: either the photon interacts directly with a parton in the proton (the direct process) or the photon acts as a source of partons which scatter off those in the proton (the resolved process). The first year of HERA operation led to the observation of hard scattering in γp collisions with evidence for multijet structure as well as the presence of the resolved process [3,4]. Measurements of dijet events allowed the separation of the resolved and direct processes [5]. The jet profiles have been measured and found to be described by leading-logarithm parton-shower calculations, except for resolved processes in the forward region [6–8].

In this paper, the internal structure of photoproduced jets is studied at the hadron level. The investigation of the internal structure of jets gives insight into the transition between a parton produced in a hard process and the experimentally observable spray of hadrons. In the present study, jets are searched for with an iterative cone algorithm [9,10] with radius $R = 1$ in the pseudorapidity[1] (η) - azimuth (ϕ) plane. The jet shape is defined as the average fraction of the jet's transverse energy (E_T^{jet}) that lies inside an inner cone of radius r concentric with the jet defining cone [11]:

$$\psi(r) = \frac{1}{N_{jets}} \sum_{jets} \frac{E_T(r)}{E_T(r = R)} \qquad (1)$$

where $E_T(r)$ is the transverse energy within the inner cone of radius r and N_{jets} is the total number of jets in the sample. By definition, $\psi(r = R) = 1$.

The jet shape, $\psi(r)$, is determined by fragmentation and gluon radiation. However, at sufficiently high E_T^{jet} the most important contribution is predicted to come from hard gluon emission off the primary parton and, therefore, is calculable in perturbative QCD. The lowest-non-trivial order contribution to the jet shape is given by next-to-leading order (NLO) QCD calculations for the reaction $AB \to \text{jet} + X$. Perturbative QCD predicts that gluon jets are broader than quark jets as a consequence of the fact that the gluon-gluon is larger than the quark-gluon coupling strength.

Measurements of jet shapes have been made in $\bar{p}p$ collisions at $\sqrt{s} = 1.8$ TeV using only charged particles [12] as well as both neutral and charged particles [13], and a qualitative agreement with NLO QCD calculations [11, 14] was found. Similar measurements have been made in

176.07/95
[25] now a self-employed consultant
[26] supported by an EC fellowship
[27] PPARC Post-doctoral Fellow
[28] now at Osaka Univ., Osaka, Japan
[29] supported by JSPS Postdoctoral Fellowships for Research Abroad
[30] now at Wayne State University, Detroit
[31] partially supported by Comunidad Autonoma Madrid
[32] partially supported by the Foundation for German-Russian Collaboration DFG-RFBR
(grant no. 436 RUS 113/248/3 and no. 436 RUS 113/248/2)
[33] now at Department of Energy, Washington
[34] supported by the Feodor Lynen Program of the Alexander von Humboldt foundation
[35] Glasstone Fellow
[36] supported by a MINERVA Fellowship
[37] now at ICEPP, Univ. of Tokyo, Tokyo, Japan
[38] present address: Tokyo Metropolitan College of Allied Medical Sciences, Tokyo 116, Japan
[39] supported by the Polish State Committee for Scientific Research, grant No. 2P03B09308
[40] supported by the Polish State Committee for Scientific Research, grant No. 2P03B09208
[a] supported by the Natural Sciences and Engineering Research Council of Canada (NSERC)
[b] supported by the FCAR of Québec, Canada
[c] supported by the German Federal Ministry for Education and Science, Research and Technology (BMBF), under contract numbers 057BN19P, 057FR19P, 057HH19P, 057HH29P, 057SI75I
[d] supported by the MINERVA Gesellschaft für Forschung GmbH, the German Israeli Foundation, and the U.S.-Israel Binational Science Foundation
[e] supported by the German Israeli Foundation, and by the Israel Science Foundation
[f] supported by the Italian National Institute for Nuclear Physics (INFN)
[g] supported by the Japanese Ministry of Education, Science and Culture (the Monbusho) and its grants for Scientific Research
[h] supported by the Korean Ministry of Education and Korea Science and Engineering Foundation
[i] supported by the Netherlands Foundation for Research on Matter (FOM)
[j] supported by the Polish State Committee for Scientific Research, grant No. 115/E-343/SPUB/P03/002/97, 2P03B10512, 2P03B10612, 2P03B14212, 2P03B10412
[k] supported by the Polish State Committee for Scientific Research (grant No. 2P03B08308) and Foundation for Polish-German Collaboration
[l] partially supported by the German Federal Ministry for Education and Science, Research and Technology (BMBF)
[m] supported by the Fund for Fundamental Research of Russian Ministry for Science and Education and by the German Federal Ministry for Education and Science, Research and Technology (BMBF)
[n] supported by the Spanish Ministry of Education and Science through funds provided by CICYT
[o] supported by the Particle Physics and Astronomy Research Council
[p] supported by the US Department of Energy
[q] supported by the US National Science Foundation

[1] The ZEUS coordinate system is defined as right-handed with the Z-axis pointing in the proton beam direction, hereafter referred to as forward, and the X-axis horizontal, pointing towards the centre of HERA. The pseudorapidity is defined as $\eta = -\ln(\tan\frac{\theta}{2})$, where the polar angle θ is taken with respect to the proton beam direction

e^+e^- interactions at LEP1 using both neutral and charged particles [15] and found to be well described by leading-logarithm parton-shower Monte Carlo calculations. It was observed [15] that the jets in e^+e^- are significantly narrower than those in $\bar{p}p$. This is due to the different mixtures of quark and gluon jets in these two environments [15]. Measurements of the jet width at LEP1 have shown that gluon jets are indeed broader than quark jets [16].

In this paper, measurements are presented of the jet shapes in both inclusive jet and dijet photoproduction at centre-of-mass energies in the range $134 - 277$ GeV. The data sample used in this analysis was collected with the ZEUS detector in e^+p interactions at the HERA collider and corresponds to an integrated luminosity of 2.65 pb^{-1}. Jets are selected with $E_T^{jet} > 14$ GeV and $-1 < \eta^{jet} < 2$. The jet shape is measured using the ZEUS calorimeter and corrected to the hadron level. The measurements are presented as a function of the jet transverse energy and pseudorapidity. In dijet photoproduction, the jet shapes are measured for resolved and direct processes defined by the fraction of the photon's momentum participating in the production of the two jets of highest E_T^{jet}.

Measurements of jet shapes are compared to QCD calculations based on different approaches:

1) LO QCD calculation including initial and final state QCD radiation in the leading-logarithm parton-shower approximation as implemented in the program PYTHIA 5.7 [17]. The final state parton system is hadronised using the LUND string model [18].
2) LO QCD calculation as implemented in the program PYTHIA without initial and final parton radiation. The final state parton system is hadronised using the LUND string model.
3) Fixed-order perturbative QCD calculation of the reaction $e^+p \to 3\,\text{partons} + X$ [19,20]. Fragmentation effects are not included.

These comparisons allow the study of the relative importance of parton radiation and fragmentation in the formation of a jet as well as the differences between quark and gluon jets. It should be noted that the first two predictions refer to the hadron level while the third refers to the parton level. For the first two predictions, jets are searched for in the final state hadronic system using the same jet algorithm as in the data. For the third prediction, the experimental jet algorithm has been simulated by the introduction of an additional parameter, R_{SEP}, as proposed in [11].

2 Experimental conditions

During 1994 HERA operated with 153 colliding bunches of protons of energy $E_p = 820$ GeV and positrons of energy $E_e = 27.5$ GeV, with 96 ns between bunch crossings.

A description of the ZEUS detector can be found in [21, 22]. The components used in this analysis are briefly discussed. The uranium-scintillator calorimeter (CAL) [23] covers 99.7% of the total solid angle. It consists of the forward calorimeter (FCAL) covering the range $2.6° < \theta < 36.7°$ in polar angle, the barrel calorimeter (BCAL) covering $36.7° < \theta < 129.1°$, and the rear calorimeter (RCAL) covering $129.1° < \theta < 176.2°$. Holes of 20×20 cm^2 in the centre of FCAL and RCAL are required to accommodate the HERA beampipe. For normal incidence, the depth of the CAL is 7 interaction lengths in FCAL, 5 in BCAL and 4 in RCAL. Each of the calorimeter parts is subdivided into towers which in turn are segmented longitudinally into one electromagnetic (EMC) and one (RCAL) or two (FCAL, BCAL) hadronic (HAC) sections. The sections are further subdivided into cells of inner-face sizes of approximately 5×20 cm^2 (10×20 cm^2 in the RCAL) for the EMC and 20×20 cm^2 for the HAC sections. Each cell is viewed by two photomultipliers. At $\theta = 90°$ the size of an EMC (HAC) cell in the $\eta - \phi$ plane is approximately $0.04 \times 11°$ ($0.16 \times 11°$). Under test beam conditions the calorimeter has an energy resolution of $\sigma/E = 18\%/\sqrt{E(\text{GeV})}$ for electrons and $\sigma/E = 35\%/\sqrt{E(\text{GeV})}$ for hadrons. In order to minimise the effects of noise due to the uranium radioactivity, all EMC (HAC) cells with an energy deposit of less than 60 (110) MeV are discarded in the analysis. For isolated energy deposits, consisting of one cell surrounded by empty cells, this cut was increased to 100 (150) MeV. Particles impinging on the CAL lose energy in the inactive material in front of the CAL. In the region relevant for the present analysis, the inactive material constitutes about one radiation length except in the region around the rear beampipe, $\theta \gtrsim 170°$, and the solenoid support structure, $25° \lesssim \theta \lesssim 45°$ and $130° \lesssim \theta \lesssim 145°$, where it is up to 2.5 radiation lengths. For the following measurements, the transverse energy and the shape of the jets have been corrected for these energy losses (see Sect. 5).

The tracking system consists of a vertex detector (VXD) [24], a central tracking chamber (CTD) [25], and a rear tracking detector (RTD) [22] enclosed in a 1.43 T solenoidal magnetic field. The interaction vertex is measured with a typical resolution along (transverse to) the beam direction of 0.4 (0.1) cm.

Proton-gas events occurring upstream of the nominal interaction point are out of time with respect to the e^+p interactions and are rejected by timing measurements using a set of scintillation counters.

2.1 Trigger conditions

The ZEUS detector uses a three-level trigger system [22]. At the first level events were triggered on a coincidence of a regional or transverse energy sum in the CAL and at least one track from the interaction point measured in the CTD. At the second level a total transverse energy of at least 8 GeV, excluding the energy in the eight CAL towers immediately surrounding the forward beampipe, was required, and cuts on CAL energies and timing were used to suppress events caused by interactions between the proton beam and residual gas in the beampipe.

The full event information was available at the third-level trigger (TLT). Tighter timing cuts as well as algo-

rithms to remove beam-halo muons and cosmic muons were applied. For this analysis, the following additional conditions were required: a) the event has a vertex reconstructed by the tracking chambers with the Z value in the range $|Z| < 60$ cm; b) $E - p_Z \geq 8$ GeV, where E is the total energy as measured by the CAL, $E = \sum_i E_i$, and p_Z is the Z-component of the vector $\mathbf{p} = \sum_i E_i \mathbf{r}_i$; in both cases the sum runs over all CAL cells, E_i is the energy of the calorimeter cell i and $\mathbf{r}_i$ is a unit vector along the line joining the reconstructed vertex and the geometric centre of the cell i; c) $p_Z/E \leq 0.95$ to reject beam-gas interactions (this cut was not applied for events with $E - p_Z \geq 12$ GeV); and d) the total transverse energy as measured by the CAL, excluding the cells with polar angles below 10°, exceeds 20 GeV.

For studies of the trigger efficiency an additional sample of events was selected by the TLT based upon jets found using a cone algorithm with radius $R = 1$ applied to the CAL cell energies and positions. The events were required to fulfill the same conditions a), b) and c) as above, and to have at least one jet of transverse energy, as measured by the CAL, $E^{jet}_{T,cal} > 6.5$ GeV and $\eta^{jet}_{cal} < 2.5$.

3 Data selection

Events from quasi-real photon proton collisions containing jets were selected offline using similar criteria as reported previously [6]. The main steps are briefly discussed here. A search for jet structure using the CAL cells (see Sect. 5) is performed, and events with at least one jet of transverse energy, as measured by the CAL, $E^{jet}_{T,cal} > 10$ GeV and $-1 < \eta^{jet}_{cal} < 2$ are retained. The contamination from beam-gas interactions, cosmic showers and halo muons is negligible after demanding: a) at least two tracks pointing to the vertex; b) the vertex position along the beam axis to lie in the range -29 cm $< Z < 36$ cm; c) less than five tracks not associated with the vertex and compatible with an interaction upstream in the direction of the proton beam; d) the number of tracks not associated with the vertex be less than 10% of the total number of tracks; and e) the total missing transverse momentum ($\not{p}_T$) be small compared to the total transverse energy (E^{tot}_T) by requiring $\not{p}_T/\sqrt{E^{tot}_T} < 2$ GeV$^{\frac{1}{2}}$. Deep inelastic e^+p scattering (DIS) neutral current events with an identified scattered positron candidate in the CAL according to the algorithm described in [5] are removed from the sample.

The selected sample consists of events from e^+p interactions with $Q^2 \leq 4$ GeV^2 and a median of $Q^2 \approx 10^{-3}$ GeV^2. The γp centre-of-mass energy (W) is calculated using the expression $W = \sqrt{ys}$, where y is the inelasticity variable and s is the squared e^+p centre-of-mass energy (300^2 GeV^2). The event sample is restricted to the kinematic range $0.2 < y < 0.85$ using the following procedure. The method of Jacquet-Blondel [26], $y_{JB} = (E - p_Z)/(2E_e)$, is used to estimate y from the energies measured in the CAL cells. Due to the energy lost in the inactive material in front of the CAL and to particles lost in the rear beampipe, y_{JB} systematically underestimates the true y by approximately 20%, an effect which is adequately reproduced in the Monte Carlo simulation of the detector. To compensate for this deficiency, the event selection required $0.16 < y_{JB} < 0.7$. The data sample consists of 15,368 events with a total of 18,897 jets. The only significant remaining background is from unidentified DIS neutral current interactions with $Q^2 > 4$ GeV^2, which is estimated by Monte Carlo techniques to be below 2%.

4 Monte Carlo simulation

The response of the detector to jets and the correction factors for the jet shapes were determined from samples of Monte Carlo events.

The programs PYTHIA 5.7 [17] and HERWIG 5.8 [27] were used to generate photoproduction events for resolved and direct processes. In PYTHIA the positron-photon vertex was modelled according to the Weizsäcker-Williams approximation. In the case of HERWIG, the exact matrix elements were used for direct processes ($e^+g \to e^+q\bar{q}$ and $e^+q \to e^+qg$) and the equivalent photon approximation for resolved processes. Events were generated using GRV-HO [28] for the photon parton distributions and MRSA [29] for the proton parton distributions. In both generators, the partonic processes were simulated using LO matrix elements, with the inclusion of initial and final state parton showers. Fragmentation into hadrons was performed using the LUND string model [18] as implemented in JETSET [30] in the case of PYTHIA, and the cluster model in the case of HERWIG. Samples of events were generated with different values of the cutoff on the transverse momentum of the two outgoing partons, starting at $\hat{p}_{Tmin} = 8$ GeV.

Additional samples of events were generated using the option of multiparton interactions (MI) in PYTHIA. This option, which applies only to resolved processes, adds interactions between the partons in the proton and the photon remnants calculated as LO QCD processes to the hardest scattering process of the event. The PYTHIA MI events were generated with a cutoff for the effective minimum transverse momentum for multiparton interactions of 1.0 GeV and with a cutoff on the transverse momentum of the two outgoing partons from the hardest scattering of $\hat{p}_{Tmin} = 8$ GeV.

All generated events were passed through the ZEUS detector and trigger simulation programs [22]. They were reconstructed and analysed by the same program chain as the data.

5 Jet search and reconstruction of the jet shape

An iterative cone algorithm in the $\eta - \phi$ plane [9,10] (PUCELL) is used to reconstruct jets, from the energy measured in the CAL cells for both data and simulated events, and also from the final state hadrons for simulated events.

The procedure is explained in detail for the jet reconstruction from the CAL cell energies (*cal* jets). In a first

step, each CAL cell with a transverse energy in excess of 300 MeV is considered as a seed for the search. Their corresponding $\eta-\phi$ values are obtained from the unit vectors joining the vertex of the interaction and the geometric centres of the cells. The seeds are then combined into preclusters starting from that with highest transverse energy if their distance in the $\eta-\phi$ plane, $\sqrt{(\Delta\eta)^2+(\Delta\phi)^2}$, is smaller than 1 unit. The axis of the precluster is defined according to the Snowmass convention [10], where $\eta^{precluster}$ ($\phi^{precluster}$) is the transverse-energy weighted mean pseudorapidity (azimuth) of all the seeds belonging to that precluster.

In a second step, a cone of radius $R = 1$ is drawn around each precluster and all the CAL cells within that cone are combined to form a cluster. The axis of the cluster is defined according to the same prescription as for the preclusters but including all the CAL cells belonging to that cluster. A new cone of $R = 1$ is then drawn around the axis of the resulting cluster. All cells with geometric centres inside the cone are used to recalculate a new cluster axis. The procedure is iterated until the content of the cluster remains unchanged.

In a third step, the energy sharing of overlapping clusters is considered. Two clusters are merged if the overlapping energy exceeds 75% of the total energy of the cluster with the lower energy; otherwise two different clusters are formed and the common cells are assigned to the nearest cluster. Finally, a cluster is called a jet if the transverse energy as measured by the CAL, $E^{jet}_{T,cal}$, exceeds 10 GeV. The angular variables associated with the *cal* jets are denoted by η^{jet}_{cal} and ϕ^{jet}_{cal}.

The following procedure was used to reconstruct the jet shape from the CAL cells: for each jet the sum of the transverse energies of the CAL cells assigned to the jet with a distance $r' = \sqrt{(\Delta\eta)^2+(\Delta\phi)^2}$ to the jet axis smaller than r is determined, $E_{T,cal}(r)$, and divided by $E_{T,cal}(r=1)$. The jet shape as measured with the CAL, $\psi_{cal}(r)$, is thus defined as:

$$\psi_{cal}(r) = \frac{1}{N_{jets}} \sum_{jets} \frac{E_{T,cal}(r)}{E_{T,cal}(r=1)}, \qquad (2)$$

where the sum runs over all the jets in the selected sample and N_{jets} is the total number of jets in the sample.

For the Monte Carlo events, the same jet algorithm is also applied to the final state particles. In this search, all particles with lifetimes longer than 10^{-13} s and with polar angles between 5° and 175° are considered. The jets found are called *hadron* jets and the variables associated with them are denoted by $E^{jet}_{T,had}$, η^{jet}_{had}, and ϕ^{jet}_{had}. *Hadron* jets with $E^{jet}_{T,had} > 14$ GeV and $-1 < \eta^{jet}_{had} < 2$ are selected. The same jet shape definition as used above for the CAL cells is applied to the final state particles in the case of simulated events and the resulting jet shape is denoted by $\psi^{MC}_{had}(r)$.

The comparison of the reconstructed jet variables between the *hadron* and the *cal* jets in simulated events [6] shows no significant systematic shift in the angular variables η^{jet}_{cal} and ϕ^{jet}_{cal} with respect to η^{jet}_{had} and ϕ^{jet}_{had}. However, the transverse energy of the *cal* jet underestimates that of the *hadron* jet by an average amount of $\approx 16\%$ with an r.m.s. of 11%. The transverse energy corrections to *cal* jets averaged over the azimuthal angle were determined using the Monte Carlo events [6]. These corrections are constructed as multiplicative factors, $C(E^{jet}_{T,cal}, \eta^{jet}_{cal})$, which, when applied to the E_T of the *cal* jets give the 'corrected' transverse energies of the jets, $E^{jet}_T = C(E^{jet}_{T,cal}, \eta^{jet}_{cal}) \times E^{jet}_{T,cal}$ [6]. These corrections mainly take into account the energy losses due to the inactive material in front of the CAL.

5.1 Jet shape corrections

The jet shapes as measured with the CAL are corrected to the hadron level using the Monte Carlo event samples. The corrected jet shapes are denoted by $\psi(r)$ and refer to jets at the hadron level with a cone radius of one unit in the $\eta-\phi$ plane. The measurements are given for jets of corrected transverse energy $E^{jet}_T > 14$ GeV and $-1 < \eta^{jet} < 2$, and in the kinematic region defined by $Q^2 \leq 4$ GeV^2 and $134 < W < 277$ GeV.

The reconstructed jet shapes are corrected for acceptance and smearing effects using the samples of Monte Carlo events of resolved and direct processes. The correction factors also take into account the efficiency of the trigger, the selection criteria, the purity and efficiency of the jet reconstruction, and the effects of energy losses due to the inactive material in front of the CAL. The corrected jet shapes are determined bin-by-bin as $\psi(r) = F^{MC}_{cal}(r) \cdot \psi_{cal}(r)$, where the correction factors $F^{MC}_{cal}(r)$ are defined as $F^{MC}_{cal}(r) = \psi^{MC}_{had}(r)/\psi^{MC}_{cal}(r)$. $F^{MC}_{cal}(r)$ is determined separately for each interval in η^{jet} and E^{jet}_T.

For this approach to be valid, the uncorrected jet shapes in the data must be described by the Monte Carlo simulations at the detector level. As shown later, this condition is in general satisfied by both the PYTHIA and HERWIG simulations although some disagreement is observed in the forward region in the case of inclusive jet production. The latter can be reduced by adjusting the relative contribution of direct processes and the fraction of gluon jets in both resolved and direct processes. In the simulated events a *cal* jet is classified as a quark or gluon jet depending on the type (quark or gluon) of the closest parton from the two-to-two hard subprocess.

The following procedure was adopted to obtain the best description of the uncorrected jet shapes: a) the relative contributions of resolved and direct processes were tuned by a fit to the measured RCAL energy distribution in the data; a distinct distribution of the energy deposit in the rear direction for resolved (direct) processes is expected due to the presence (absence) of the photon remnant; b) the fraction of gluon jets in direct and resolved processes was adjusted by a fit to the uncorrected jet shape. This procedure was applied separately for each η^{jet} and E^{jet}_T interval. The correction factors $F^{MC}_{cal}(r)$ are taken from this tuned version of PYTHIA. For the com-

parisons to the measurements presented in Sects. 6 and 7 the untuned version of PYTHIA has been used.

The correction factors do not show a strong dependence on η^{jet} or E_T^{jet} and differ from unity by less than 10% (5%) for $r \geq 0.4$ ($r \geq 0.6$). For $r = 0.3$ ($r = 0.2$) they can increase to 15% (30%). The dependence of the correction factors on the choice of fragmentation scheme, relative contributions of direct and resolved processes, fractions of gluon and quark jets in each process, and the inclusion of multiparton interactions in resolved processes was studied and found to be small. The resulting differences are taken into account as contributions to the total systematic uncertainty assigned to the measurements reported in the next sections.

5.2 Systematic uncertainties of the measurements

A detailed study of the sources contributing to the systematic uncertainties of the measurements was carried out. For each source, the largest change in the corrected value of $\psi(r)$ (indicated in parentheses) at a fixed value of r typically occurs at $r = 0.2$ and the magnitude of the induced change decreases rapidly as r increases:

- The correction functions to the jet shapes were calculated using the event samples of the untuned version of PYTHIA (± 3%).
- Using the HERWIG generator to evaluate the energy corrections to the jets and the correction functions to the jet shapes (± 5%).
- The correction functions were calculated using Monte Carlo samples of PYTHIA events consisting exclusively of either gluon or quark jets (± 9%).
- The use of the PYTHIA generator including multiparton interactions in resolved processes (± 4%).
- Variation of the absolute energy scale of the CAL in the simulated events by ± 3% (± 2%).
- The uncertainty in the simulation of the CAL response to low-energy particles (−2%).
- Uncertainties in the simulation of the trigger and variation of the cuts used to select the data within the ranges allowed by the comparison between data and Monte Carlo simulations resulted in negligible changes in the corrected jet shapes.

The systematic uncertainties for different values of r are correlated. For all the results the statistical errors are negligible compared to the systematic uncertainties. The total positive (negative) systematic uncertainty on $\psi(r)$ at each value of r was determined by adding in quadrature the positive (negative) deviations from the central value. The systematic uncertainties were then added in quadrature to the statistical errors and are shown as error bars in the figures.

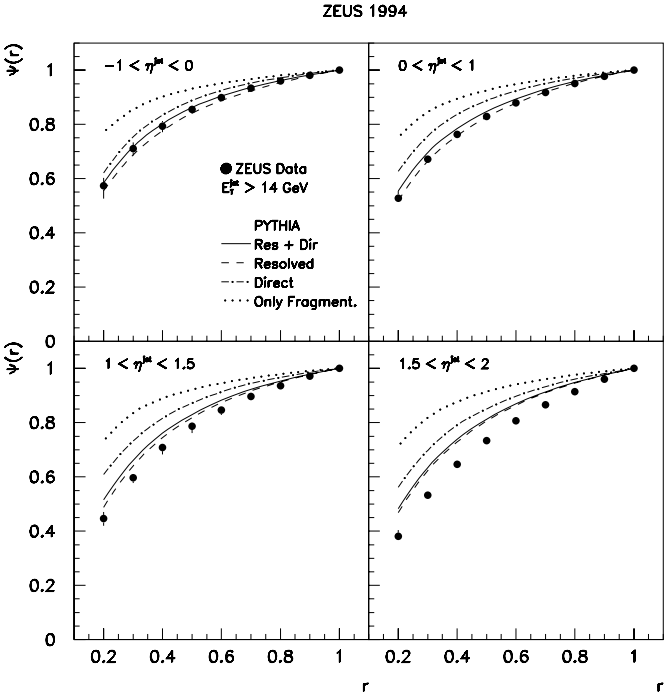

Fig. 1. The measured jet shapes corrected to the hadron level, $\psi(r)$, for jets in the E_T^{jet} range above 14 GeV in different η^{jet} regions. The *error bars* show the statistical and systematic errors added in quadrature. For comparison, the predictions of PYTHIA for resolved (*dashed*), direct (*dot-dashed line*), and resolved plus direct processes (*solid line*) are shown. The predictions of PYTHIA for resolved plus direct processes without initial and final state parton radiation (*dotted line*) are also included (labelled by 'Only Fragment.')

6 Inclusive jet photoproduction results

6.1 Jet pseudorapidity dependence of the jet shape

The jet shape for jets with $E_T^{jet} > 14$ GeV is presented in Fig. 1 for four different η^{jet} regions. It is observed that the jet shape broadens as η^{jet} increases. In the following the predictions of the PYTHIA generator are compared to the measurements. The predictions using HERWIG are very similar to those of PYTHIA and lead to the same conclusions.

Comparison to parton shower model predictions

The predictions of PYTHIA for direct, resolved, and direct plus resolved processes are compared to the measured jet shapes in Fig. 1. The admixture of the two processes was chosen according to the cross sections as given by PYTHIA. The dependence of the predictions on the specific sets of proton or photon parton distributions is negligible. The measured jet shapes in the range $-1 < \eta^{jet} < 1$ are reasonably well described by the predictions of PYTHIA for either resolved plus direct or resolved processes alone. The predicted jet shapes in direct processes are significantly narrower than those of the data. These results are in agreement with the dominance of resolved processes in the E_T^{jet} range studied, as observed

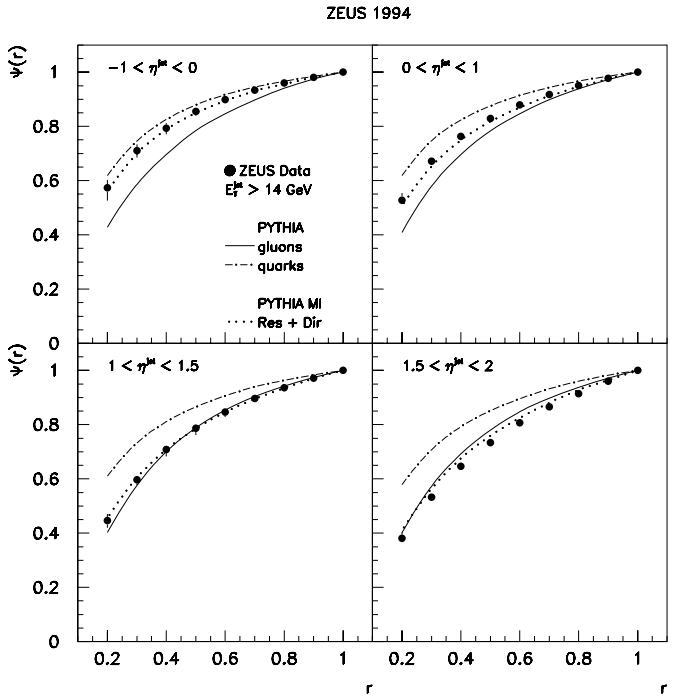

Fig. 2. The measured jet shapes corrected to the hadron level, $\psi(r)$, for jets in the E_T^{jet} range above 14 GeV in different η^{jet} regions. The *error bars* show the statistical and systematic errors added in quadrature. For comparison, the predictions of PYTHIA including resolved plus direct processes for quark (*dot-dashed line*) and gluon jets (*solid line*), and those of PYTHIA MI for resolved plus direct processes (*dotted line*) are shown

in the measurement of the inclusive jet differential cross sections [6,31]. As η^{jet} increases beyond $\eta^{jet} = 1$, the predicted jet shapes increasingly deviate from those in the data, which are significantly broader in the most forward region ($1.5 < \eta^{jet} < 2$).

In order to study the relative importance of parton radiation and fragmentation effects, the predictions of PYTHIA for resolved plus direct processes without initial and final state parton radiation are also shown in Fig. 1. Since the predicted jet shapes based on fragmentation only are significantly narrower than the measured ones, it is concluded that, at the transverse energies studied here, the shape of jets is mainly dictated by parton radiation and cannot be explained by hadronisation alone.

Comparison to the parton shower model predictions of quark and gluon jets

The difference between quark and gluon jets is modelled in PYTHIA by a leading-logarithm parton-shower approximation. The jet shapes, as predicted by PYTHIA, for quark and gluon jets are shown separately in Fig. 2, together with the same data as in Fig. 1. The predictions of PYTHIA for the two types of jets are computed separately for resolved and direct processes, and then averaged according to the cross sections given by PYTHIA. The predicted jet shapes are broader for gluon jets than for quark jets in each region of η^{jet} and exhibit only a small dependence on η^{jet}.

The differences in the predictions for resolved and direct processes (see Fig. 1) come mainly from the different fractions of quark and gluon jets in the final state depending on the η^{jet} region. This difference, in turn, originates from the different dominant two-body subprocesses. In the case of direct processes, where the dominant subprocess is photon-gluon fusion $\gamma g \to q\bar{q}$, PYTHIA predicts the fraction of quark jets to be 80-100% depending on η^{jet}. In the case of resolved processes, the dominant subprocess in the kinematic regime studied is $q_\gamma g_p \to qg$ and the predicted fraction of quark jets has a stronger η^{jet}-dependence: from $\sim 80\%$ at $\eta^{jet} = -1$ to $\sim 40\%$ at $\eta^{jet} = 2$. The comparison of measurement and prediction (see Fig. 2) shows that the broadening of the jet shapes in the data as η^{jet} increases is consistent with an increasing fraction of gluon jets. Therefore, one possible reason for the deviation between data and prediction is an underestimation of the fraction of gluon jets in the region $\eta^{jet} > 1$ by PYTHIA.

Comparison to model predictions including multiparton interactions

An excess of transverse energy outside of the jet cone for jets with $\eta^{jet} > 1$ with respect to the expectations of PYTHIA was observed in previous studies [6,31]. Since this excess may have some effect on the comparisons discussed so far, its influence on the jet shape has been considered. In order to simulate an increased energy flow the PYTHIA generator including MI was used; the cutoff (1.0 GeV) for the effective minimum transverse momentum for MI was tuned to reproduce the transverse energy flow outside of the jet cone in the data. The jet shapes predicted by PYTHIA MI are also shown in Fig. 2. Comparing with Fig. 1, it is observed that the effects of MI on the jet shape are very small in the region $-1 < \eta^{jet} < 1$, increase gradually with η^{jet} and yield an improved description of the data in the region $\eta^{jet} > 1$. The differences in the predicted jet shapes between PYTHIA and PYTHIA MI are considered as an estimate of the uncertainty in the simulation of the energy flow outside the jet cone due to a possible underlying event. The conclusions that the measured jet shapes are consistent with the dominance of resolved processes and that the parton radiation is the main mechanism responsible for the jet shape still hold when this uncertainty is taken into account.

Comparison to model predictions for fixed r

Figure 3 shows the measured jet shape at a fixed value of $r = 0.5$, $\psi(r = 0.5)$, as a function of η^{jet}. The predictions of PYTHIA for quark jets with and without MI span a band above the data, while those for gluon jets with and without MI span a band typically below the data. It is also seen that the effect of MI is larger as η^{jet} increases. The predictions for resolved plus direct processes are also shown in Fig. 3. The prediction of PYTHIA fails to describe the relatively strong broadening of the measured jet shape for $\eta^{jet} > 1$. As mentioned earlier, one reason might be that the fraction of gluon jets in the region $\eta^{jet} > 1$ is underestimated. However, when the effects of a possible

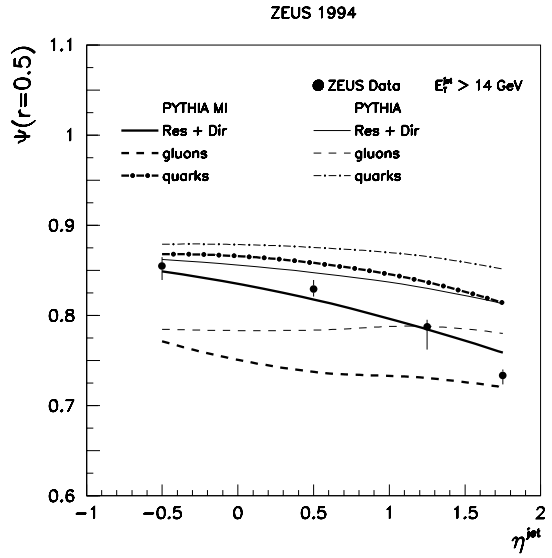

Fig. 3. The measured jet shape corrected to the hadron level at a fixed value of $r = 0.5$, $\psi(r = 0.5)$, as a function of η^{jet} for jets with E_T^{jet} larger than 14 GeV. The *error bars* show the statistical and systematic errors added in quadrature. For comparison, various predictions of PYTHIA including resolved plus direct processes are shown: quark jets (*thin dot-dashed line*), gluon jets (*thin dashed line*) and all jets (*thin solid line*). The corresponding predictions of PYTHIA MI are displayed with *thick lines*

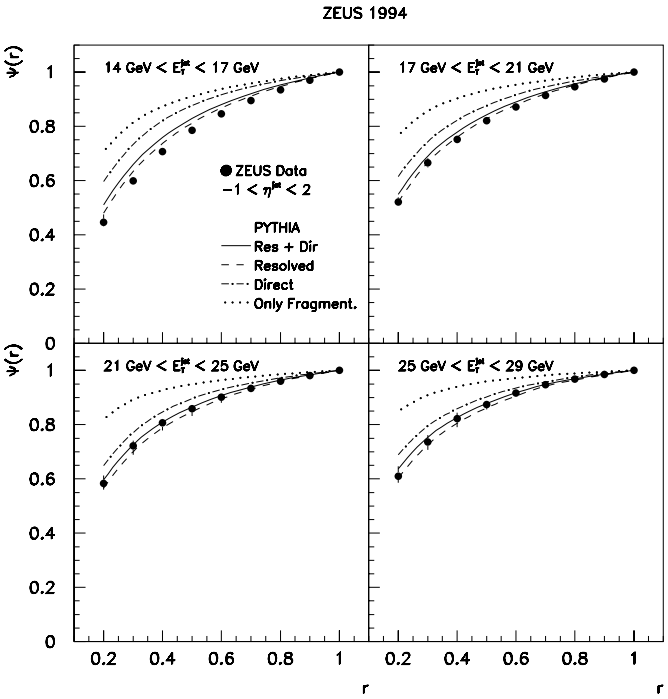

Fig. 4. The measured jet shapes corrected to the hadron level, $\psi(r)$, for jets in the η^{jet} range between -1 and 2 in different E_T^{jet} regions. The *error bars* show the statistical and systematic errors added in quadrature. For comparison, the predictions of PYTHIA for resolved (*dashed*), direct (*dot-dashed line*), and resolved plus direct processes (*solid line*) are shown. The predictions of PYTHIA for resolved plus direct processes without initial and final state parton radiation (*dotted line*) are also included (labelled by 'Only Fragment.')

underlying event are taken into account, using PYTHIA MI, the measured broadening in the forward region is accounted for with the default fraction of gluon jets. Note that, in any case, as η^{jet} increases the measured jet shape changes from a value close to the upper band (quark jets) to a value within the lower band (gluon jets). It is concluded that the broadening of the measured jet shape as η^{jet} increases is consistent with an increase of the fraction of gluon jets independent of the effects of a possible underlying event.

6.2 E_T^{jet} dependence of the jet shape

The E_T^{jet} dependence of the jet shape is presented in Fig. 4. It is observed that the jets become narrower as E_T^{jet} increases. For $E_T^{jet} > 17$ GeV the predictions of PYTHIA for resolved or resolved plus direct processes reproduce the data reasonably well. In the lowest E_T^{jet} region, differences between data and the predictions are observed. Again the predicted jet shapes for direct processes are narrower than for the data. PYTHIA including resolved plus direct processes, but without initial and final state parton radiation, predicts jet shapes which are too narrow in each region of E_T^{jet}. These comparisons show again that parton radiation is the dominant mechanism responsible for the jet shape in the whole range of E_T^{jet} studied.

The measured jet shape at a fixed value of $r = 0.5$, $\psi(r = 0.5)$, shows a moderate increase with E_T^{jet}, as seen in Fig. 5. Note that the jet shapes have been measured in ranges of E_T^{jet} and the data points in Fig. 5 are located at the weighted mean in each E_T^{jet} range. The predictions for the dependence of the jet shape on E_T^{jet} in resolved processes reproduce the data except for the lowest E_T^{jet} data point. The predicted jet shape for direct processes is narrower than the data. The effects of a possible underlying event are estimated using the predictions of PYTHIA MI. The inclusion of these effects improves the description of the data in the lowest E_T^{jet} data point, but otherwise does not alter significantly the E_T^{jet}-dependence of the jet shape.

6.3 Comparison to fixed-order QCD calculations

Lowest-non-trivial order QCD calculations of the jet shapes [19,20] are compared to our measurements in Figs. 6 and 7. These predictions include resolved and direct processes, and use the CTEQ4 [32] (GRV-HO) proton (photon) parton densities. Since the jet shape is computed only to the lowest-non-trivial order[2], $O(\alpha_s)$, the predictions are subject to relatively large uncertainties due to

[2] The lowest-non-trivial order contribution to the jet shape corresponds to the NLO matrix elements of the hard interaction. The NLO contribution to the jet shape is not available due

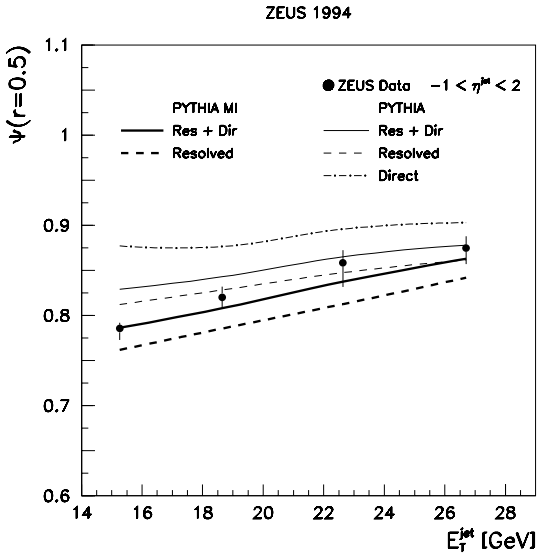

Fig. 5. The measured jet shape corrected to the hadron level at a fixed value of $r = 0.5$, $\psi(r = 0.5)$, as a function of E_T^{jet} for jets in the η^{jet} range between -1 and 2. The *error bars* show the statistical and systematic errors added in quadrature. For comparison, various predictions of PYTHIA are shown: resolved (*thin dashed line*), direct (*thin dot-dashed line*) and resolved plus direct processes (*thin solid line*). The predictions of PYTHIA MI for resolved and resolved plus direct processes are displayed with *thick lines*

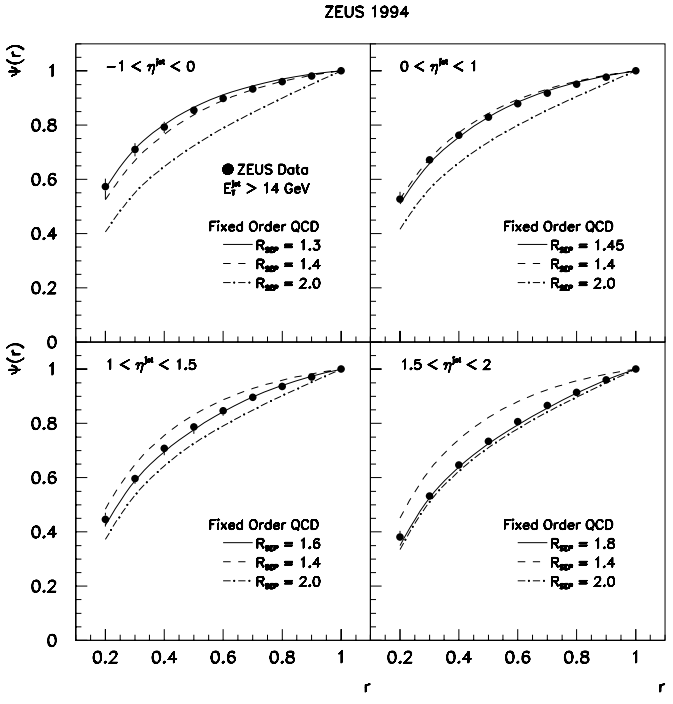

Fig. 6. The measured jet shapes corrected to the hadron level, $\psi(r)$, for jets in the E_T^{jet} range above 14 GeV in different η^{jet} regions. The *error bars* show the statistical and systematic errors added in quadrature. For comparison, the predictions for the jet shapes (*solid, dashed* and *dot-dashed lines*) based upon the fixed-order QCD calculations by M. Klasen and G. Kramer with various values of R_{SEP} (see text) are shown

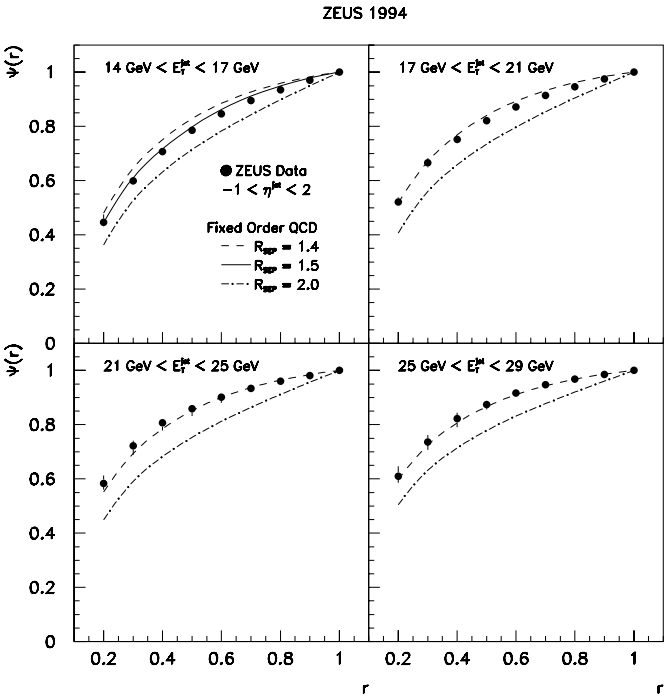

Fig. 7. The measured jet shapes corrected to the hadron level, $\psi(r)$, for jets in the η^{jet} range between -1 and 2 in different E_T^{jet} regions. The *error bars* show the statistical and systematic errors added in quadrature. For comparison, the predictions for the jet shapes (*solid, dashed* and *dot-dashed lines*) based upon the fixed-order QCD calculations by M. Klasen and G. Kramer with various values of R_{SEP} (see text) are shown

the strong dependence on the renormalisation and factorisation scales. In the calculations shown here, these scales have been chosen equal to E_T^{jet}. Since the calculations include only up to three partons in the final state, not more than two partons can build up a jet. As a result, the overlapping and merging issues of the experimental jet algorithm are not reproduced in the theoretical calculation [11,34]. An attempt was made to simulate these effects by introducing an ad-hoc R_{SEP} parameter [11]: two partons are not merged into a single jet if their separation in the $\eta - \phi$ plane is more than R_{SEP}. The calculations of the jet shape shown in Figs. 6 and 7 have been made for various R_{SEP} values[3]: for two fixed values of $R_{SEP} = 1.4$ and 2.0, and for the value of R_{SEP} which best reproduces the data [20].

The fixed-order QCD calculations with a common value of $R_{SEP} = 1.4$ reproduce reasonably well the measured jet shapes in the region $-1 < \eta^{jet} < 1$ and in the region $E_T^{jet} > 17$ GeV. In the forward region, $\eta^{jet} > 1$,

to the lack of the relevant next-to-next-to-leading order matrix elements, and in any case, as pointed out in [33], it cannot be safely calculated for the iterative cone algorithm used here

[3] Although the value $R_{SEP} = 1$ was suggested [35] for the comparison between the measurements of cross sections and theoretical calculations, other values can be used in order to match the measured jet shapes

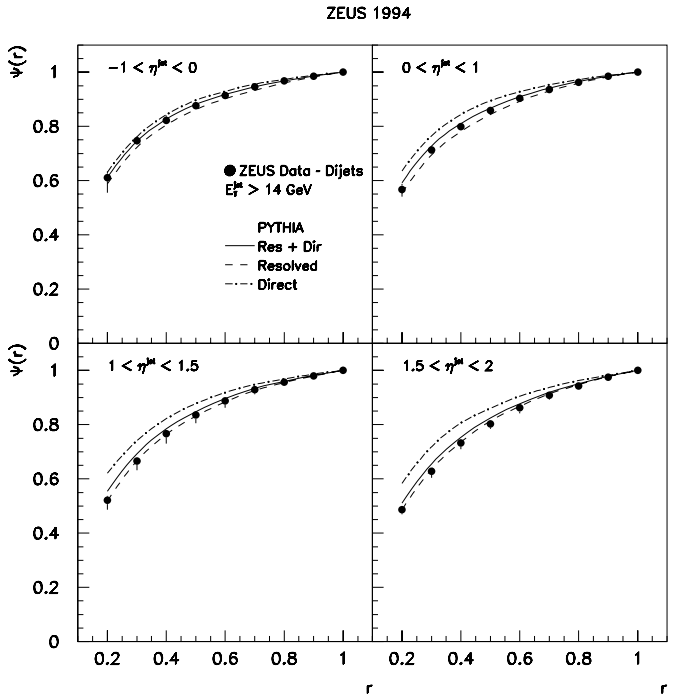

Fig. 8. The measured jet shapes corrected to the hadron level, $\psi(r)$, for each of the two highest E_T^{jet} jets in dijet photoproduction. Both jets are required to have $E_T^{jet} > 14$ GeV. The measurements are shown for four different regions in η^{jet}. The *error bars* represent the statistical and systematic errors added in quadrature. For comparison, the predictions of PYTHIA for resolved (*dashed*), direct (*dot-dashed line*), and resolved plus direct processes (*solid line*) are shown

and in the lowest E_T^{jet} region, $14 < E_T^{jet} < 17$ GeV, the calculations with $R_{SEP} = 1.4$ show significant deviations with respect to the data. The discrepancy is very similar to that observed between the predictions of PYTHIA without MI and the data. However, a satisfactory description of the data can be obtained by leaving R_{SEP} as a free parameter (for each interval in η^{jet}). A crosscheck with the data which overlaid jets from different events showed that the minimum distance at which two jets are resolved as two distinct jets depends very little on η^{jet}. Therefore, the variation of R_{SEP} with η^{jet} cannot be justified on these grounds. The use of different values of R_{SEP} to describe the data in the forward and lowest E_T^{jet} regions may be mimicking the effects of QCD higher orders and of a possible underlying event, which at present are not included in the calculations. In addition, the comparison between the measured jet shapes, which are corrected to the hadron level, and the fixed-order QCD calculations at the parton level is subject to the uncertainty of hadronisation effects.

7 Dijet photoproduction results

The jet shapes have been measured for each of the two highest E_T^{jet} jets in the reaction $ep \to \text{jet} + \text{jet} + X$. Both jets are required to have $E_T^{jet} > 14$ GeV and $-1 < \eta^{jet} < 2$. The measurements have been integrated over four non-overlapping regions in η^{jet} of each jet. The results for $\psi(r)$ are presented in Fig. 8 and are compared to the predictions of PYTHIA. The jet shape broadens as η^{jet} increases and is narrower than that of the inclusive jet sample (see Fig. 1). The predictions for resolved or resolved plus direct processes describe reasonably well the measured jet shapes in all regions of η^{jet}. The predicted jet shapes for direct processes are narrower than for the data in the region $\eta^{jet} > 0$, as expected from the dominance of resolved processes in that region. The comparison of the predicted jet shapes with the data in the region $\eta^{jet} > 1$ does not show the discrepancies observed in the inclusive jet photoproduction study. This difference is attributed to a suppression of the effects of a possible underlying event in the case of dijet events since the requirement of two high-E_T^{jet} jets increases the contribution from direct processes and, for resolved processes, decreases the leftover energy for the remnants. The broadening of the measured jet shapes in dijet photoproduction as η^{jet} increases is adequately reproduced by the predictions of PYTHIA.

In dijet photoproduction the contributions of resolved and direct processes can be separated [5,7] by using the variable:

$$x_\gamma^{OBS} = \frac{\sum_{jets} E_T^{jet} e^{-\eta^{jet}}}{2yE_e}, \qquad (3)$$

where the sum runs over the two jets of highest E_T^{jet} and yE_e is the initial photon energy. This variable represents the fraction of the photon's momentum participating in the production of the two highest E_T^{jet} jets. The LO direct and resolved processes largely populate different regions of x_γ^{OBS}, with the direct processes concentrated at high values.

The results for $\psi(r)$ are presented in Fig. 9 for both x_γ^{OBS} smaller and larger than 0.75. It is observed that the measured jet shapes for $x_\gamma^{OBS} < 0.75$ are broader than those for $x_\gamma^{OBS} \geq 0.75$. For the region of $x_\gamma^{OBS} \geq 0.75$, the jet shapes as predicted by PYTHIA including resolved plus direct processes describe well the data. The predictions of PYTHIA for the region $x_\gamma^{OBS} < 0.75$ reproduce the data reasonably well though the latter are slightly broader. The inclusion of the effects of a possible underlying event as modelled with PYTHIA MI leads to an improved description of the data in the region of $x_\gamma^{OBS} < 0.75$ and has a negligible contribution in the region of $x_\gamma^{OBS} \geq 0.75$ (not shown).

8 Summary and conclusions

Measurements of jet shapes in inclusive jet and dijet photoproduction in e^+p collisions at $\sqrt{s} = 300$ GeV using data collected by ZEUS in 1994 have been presented. The jet shapes refer to jets at the hadron level with a cone radius of one unit in the $\eta-\phi$ plane and are given in the kinematic region defined by $Q^2 \leq 4$ GeV^2 and $134 < W < 277$ GeV. Jets with $E_T^{jet} > 14$ GeV and $-1 < \eta^{jet} < 2$ have been

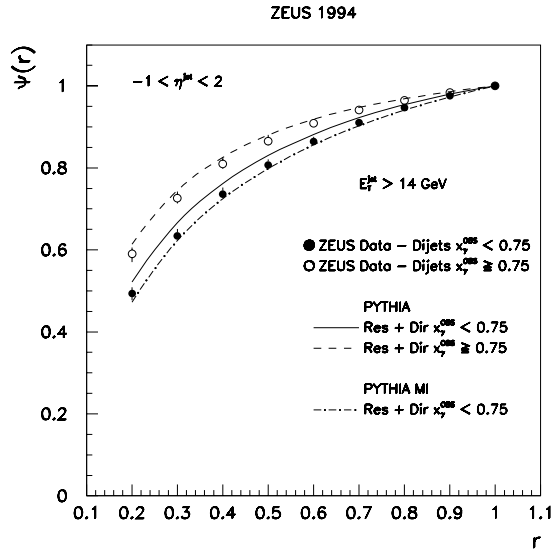

Fig. 9. The measured jet shapes corrected to the hadron level, $\psi(r)$, for each of the two highest E_T^{jet} jets in dijet photoproduction separated according to x_γ^{OBS}. Both jets are required to have $E_T^{jet} > 14$ GeV and $-1 < \eta^{jet} < 2$. The *error bars* show the statistical and systematic errors added in quadrature. For comparison, various predictions of PYTHIA including resolved plus direct processes are shown: for the region $x_\gamma^{OBS} < 0.75$ (PYTHIA without MI as the *solid line* and PYTHIA with MI as the *dot-dashed line*) and for $x_\gamma^{OBS} \geq 0.75$ (PYTHIA without MI as the *dashed line*)

considered. The dependence of the jet shapes on E_T^{jet} and η^{jet} has been studied: the jet shape broadens as η^{jet} increases and narrows as E_T^{jet} increases. In dijet photoproduction, the jet shapes have been measured separately for two regions of x_γ^{OBS}, the fraction of the photon's momentum participating in the production of the two jets of highest E_T^{jet}, $x_\gamma^{OBS} < 0.75$ and $x_\gamma^{OBS} \geq 0.75$. These subsamples are dominated by resolved and direct processes, respectively. The jet shapes in the region $x_\gamma^{OBS} < 0.75$ are systematically broader than those in the region $x_\gamma^{OBS} \geq 0.75$.

Leading-logarithm parton-shower Monte Carlo calculations of resolved and direct processes have been compared to the measured jet shapes. The predictions based on resolved or resolved plus direct processes describe reasonably well the measured jet shapes in the region $-1 < \eta^{jet} < 1$ for inclusive jet photoproduction and in the full region of η^{jet} for dijet production. The predictions including only direct processes are narrower than those measured in the data. The removal of initial and final state parton radiation in the Monte Carlo calculations gives rise to jet shapes which are too narrow compared to those of the data. The results are in agreement with the dominance of resolved processes and indicate that parton radiation is the dominant mechanism responsible for the jet shape in the E_T^{jet} range studied.

Fixed-order QCD calculations cannot reproduce the measured jet shapes over the full kinematic range with a single value of the R_{SEP} parameter.

The observed broadening of the jet shape as η^{jet} increases is consistent with an increase of the fraction of gluon jets independent of the effects of a possible underlying event.

Acknowledgements. The strong support and encouragement of the DESY Directorate has been invaluable. The experiment was made possible by the inventiveness and the diligent efforts of the HERA machine group. The design, construction and installation of the ZEUS detector have been made possible by the ingenuity and dedicated efforts of many people from inside DESY and from the home institutes who are not listed as authors. Their contributions are acknowledged with great appreciation. We would like to thank M. Klasen, G. Kramer and S.G. Salesch for valuable discussions and for providing us with their calculations.

References

1. J.F. Owens, Phys. Rev. **D21** (1980) 54
2. W.J. Stirling, Z. Kunszt in Proceedings of HERA Workshop (1987) 331; M. Drees, F. Halzen, Phys. Rev. Lett. **61** (1988) 275; M. Drees, R.M. Godbole, Phys. Rev. **D39** (1989) 169
3. H1 Collab., T. Ahmed et al., Phys. Lett. **B297** (1992) 205
4. ZEUS Collab., M. Derrick et al., Phys. Lett. **B297** (1992) 404
5. ZEUS Collab., M. Derrick et al., Phys. Lett. **B322** (1994) 287
6. ZEUS Collab., M. Derrick et al., Phys. Lett. **B342** (1995) 417
7. ZEUS Collab., M. Derrick et al., Phys. Lett. **B348** (1995) 665
8. H1 Collab., S. Aid et al., Z. Phys. **C70** (1996) 17
9. CDF Collab., F. Abe et al., Phys. Rev. **D45** (1992) 1448
10. J. Huth et al., Proc. of the 1990 DPF Summer Study on High Energy Physics, Snowmass, Colorado, edited by E.L. Berger (World Scientific, Singapore,1992) p. 134
11. S.D. Ellis, Z. Kunszt, D.E. Soper, Phys. Rev. Lett. **69** (1992) 3615
12. CDF Collab., F. Abe et al., Phys. Rev. Lett. **70** (1993) 713
13. D0 Collab., S. Abachi et al., Phys. Lett. **B357** (1995) 500
14. W.T. Giele, E.W.N. Glover, D.A. Kosower, Nucl. Phys. **B403** (1993) 633
15. OPAL Collab., R. Akers et al., Z. Phys. **C63** (1994) 197
16. OPAL Collab., G. Alexander et al., Phys. Lett. **B265** (1991) 462; OPAL Collab., P.D. Acton et al., Z. Phys. **C58** (1993) 387; OPAL Collab., R. Akers et al., Z. Phys. **C68** (1995) 179; OPAL Collab., G. Alexander et al., Z. Phys. **C69** (1996) 543; DELPHI Collab., P. Abreu et al., Z. Phys. **C70** (1996) 179; ALEPH Collab., D. Buskulic et al., Phys. Lett. **B384** (1996) 353
17. H.-U. Bengtsson, T. Sjöstrand, Comp. Phys. Comm. **46** (1987) 43; T. Sjöstrand, Comp. Phys. Comm. **82** (1994) 74
18. B. Andersson et al., Phys. Rep. **97** (1983) 31
19. G. Kramer, S.G. Salesch, Phys. Lett. **B317** (1993) 218, Phys. Lett. **B333** (1994) 519
20. M. Klasen, G. Kramer, Phys. Rev. **D56** (1997) 2702
21. ZEUS Collab., M. Derrick et al., Phys. Lett. **B293** (1992) 465

22. The ZEUS Detector, Status Report (1993), DESY 1993
23. M. Derrick et al., Nucl. Inst. Meth. **A309** (1991) 77; A. Andresen et al., Nucl. Inst. Meth. **A309** (1991) 101; A. Bernstein et al., Nucl. Inst. Meth. **A336** (1993) 23
24. C. Alvisi et al., Nucl. Inst. Meth. **A305** (1991) 30
25. N. Harnew et al., Nucl. Inst. Meth. **A279** (1989) 290; B. Foster et al., Nucl. Phys. B (Proc. Suppl.) **32** (1993) 181; B. Foster et al., Nucl. Inst. Meth. **A338** (1994) 254
26. Method proposed by F. Jacquet, A. Blondel in Proc. of the Study for an *ep* Facility for Europe, U. Amaldi et al., DESY 79/48 (1979) 377
27. G. Marchesini et al., Comp. Phys. Comm. **67** (1992) 465
28. M. Glück, E. Reya, A. Vogt, Phys. Rev. **D46** (1992) 1973
29. A.D. Martin, W.J. Stirling, R.G. Roberts, Phys. Rev. **D50** (1994) 6734
30. T. Sjöstrand, Comp. Phys. Comm. **39** (1986) 347; T. Sjöstrand, M. Bengtsson, Comp. Phys. Comm. **43** (1987) 367
31. H1 Collab., I. Abt et al., Phys. Lett. **B314** (1993) 436
32. H.L. Lai et al., Phys. Rev. **D55** (1997) 1280
33. M.H. Seymour, preprint RAL-97-026 (hep-ph/9707338)
34. W.B. Kilgore, W.T. Giele, Phys. Rev. **D55** (1997) 7183
35. J.M. Butterworth, L. Feld, M. Klasen, G. Kramer, hep-ph/9608481; Proceedings of the Workshop on "Future Physics at HERA", ed. by G. Ingelman, A. DeRoeck, R. Klanner, DESY 1996, p.554